Bio-Design and Manufacturing (2025) 8:639–655
https://doi.org/10.1631/bdm.2400107

RESEARCH ARTICLE

Engineered inflammation-induced neurodevelopmental disorders using a neurovascular-unit-on-a-chip

Rong Zou[1,2] · Zhengdi Shi[2] · Chengpan Li[2] · Fan Xu[3] · Xucai Zheng[4] · Xiaofang Du[2] · Dabing Huang[1] · Bensheng Qiu[2] · Weiping Ding[1]

Received: 20 March 2024 / Accepted: 24 November 2024

Abstract

Neuroinflammation is the primary driver and signature of many neurodevelopmental disorders. However, because neurodevelopmental disorders caused by neuroinflammation are difficult to detect at the early stage, their progression remains unclear. To date, neither animal experiments nor in vitro models have uncovered their early developmental characteristics caused by neuroinflammation. In this study, we developed a neurovascular-unit-on-a-chip (NVU-on-a-chip) to model inflammation-induced neurodevelopmental disorders. With the chip, dynamic visualization of the progression caused by neuroinflammation was clearly demonstrated, and the changes in angiogenesis and neural differentiation under neuroinflammation were replicated. In addition, the activation of astrocytes and damage to neurons and capillaries at the early stage of neurodevelopmental disorders were observed. The results revealed for the first time the structural disruption of the neurovascular units and the neurovascular coupling failure caused by neuroinflammation. Furthermore, the outcomes of anti-inflammatory intervention using ibuprofen were preliminarily demonstrated. This work provides insights into the early progression of neurodevelopmental disorders caused by neuroinflammation and offers a platform for the development of therapeutic strategies for neuroinflammation.

Rong Zou and Zhengdi Shi have contributed equally to this work.

✉ Dabing Huang
hdabing@ustc.edu.cn

✉ Bensheng Qiu
bqiu@ustc.edu.cn

✉ Weiping Ding
wpdings@ustc.edu.cn

[1] Department of Oncology, The First Affiliated Hospital of USTC, Division of Life Sciences and Medicine, University of Science and Technology of China (USTC), Hefei 230001, China

[2] School of Information Science and Technology, University of Science and Technology of China, Hefei 230027, China

[3] Anhui Province Key Laboratory of Chinese Medicinal Formula, Anhui University of Chinese Medicine, Hefei 230012, China

[4] Department of Head and Neck Surgery, West District of The First Affiliated Hospital of USTC, Division of Life Sciences and Medicine, University of Science and Technology of China, Hefei 230031, China

Graphical abstract

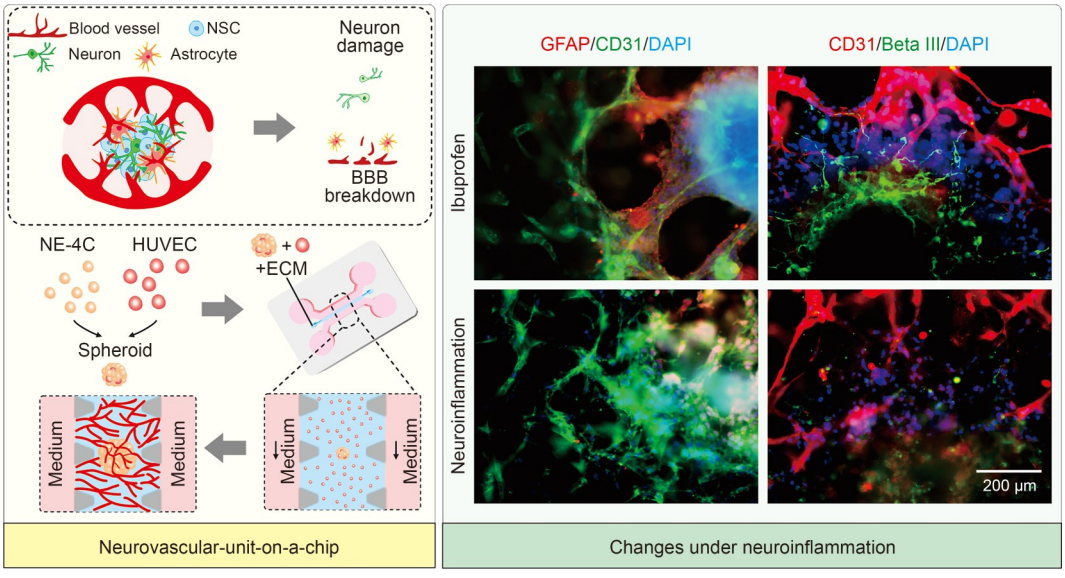

Keywords Neurovascular-unit-on-a-chip · Neuroinflammation · Neurodevelopmental disorders · Angiogenesis · Neural differentiation

1 Introduction

Neuroinflammation is the primary driver and marker of many diseases of the central nervous system [1, 2]. Many studies have indicated an association between early inflammation during the neurodevelopmental stage and neurodevelopmental disorders such as autism spectrum disorders, schizophrenia, cerebral palsy, epilepsy, cognitive impairment, and depression [3]. Neuroinflammation in the neurodevelopmental period is a dynamically complicated process [4]. The brain is particularly vulnerable during this period due to the rapid establishment of key brain processes and microvascular networks [3]. As inflammatory cytokines secreted from brain cells gradually increase, astrocyte proliferation increases, microglia activation aggravates, neuron damage accelerates, and the permeability of the blood–brain barrier (BBB) dramatically increases [5, 6]. When the complete barrier function of the brain is lost, systemic inflammatory mediators infiltrate the brain more easily, exacerbating neuroinflammation. In addition, neuroinflammatory factors that cross the BBB can circulate through the bloodstream, leading to fetal growth restriction (FGR) [5, 7]. These disturbances at the cellular level are the basis of the altered brain microstructure observed in long-term behavioral and intellectual disabilities [5]. Currently, the mechanisms of early neuroinflammation remain unclear because the development of the brain at the early stage of neuroinflammation is usually invisible. Therefore, it is necessary to develop methods to uncover the early neurodevelopmental process under neuroinflammation for its diagnosis and therapy.

A number of preclinical models have been developed to study neuroinflammation, such as animal models and in vitro models [8–10]. However, few models focus on neuroinflammation during the neurodevelopmental period. The reported animal models have used brain sections from piglets, lambs, and rats with neuroinflammation to demonstrate the disease characteristics and the effects of drugs [10–14]. For example, glial activation and neuronal damage were observed in the brains of newborn piglets with neuroinflammation [15]. Although these animal models are useful for understanding the changes in the brain under neuroinflammation, they only reveal the changes at one postnatal time point and cannot dynamically visualize disease progression [10]. In addition, brain sections can only provide structural information, which is not sufficient to reveal either the effects of neuroinflammation on angiogenesis and neural differentiation or the interactions within neurovascular units in the early stages of neural development.

Regarding in vitro models of neuroinflammation, three-dimensional (3D) models have been developed via techniques such as microfluidics [16], bioprinting, and organoids [17, 18], providing a more in vivo-like environment than two-dimensional (2D) cell culture, pushing the precision of neuroinflammation modeling to a new level [19].

Therefore, 3D models enable the observation and tracking of disease progression at the cellular level [20].

Recently, the development of a new type of 3D model, known as organ-on-a-chip, has progressed rapidly, providing new avenues for disease modeling and drug screening [21]. Brain chips, one of the extensively studied organ chips, can potentially reflect the detailed neural structure, vascular structure, and circulation of fluids in the brain. Brain chips have already been employed to replicate various diseases of the nervous system [22–25], such as prenatal exposures [26, 27] and neuroinfectious disorders [28]. Pediaditakis et al. developed a layered brain chip to investigate the disruption of the BBB caused by neuroinflammation [22]. However, studies modeling neuroinflammation and the related neurodevelopmental disorders are still very limited, and neither brain chips nor brain organoids have been reported for examining the inflammatory responses in the neurovascular unit during the neurodevelopmental period.

In this study, therefore, we developed a neurovascular-unit-on-a-chip (NVU-on-a-chip) and used it to model neuroinflammation during the neurodevelopmental period. The NVU-on-a-chip was constructed using cutting-edge organoid-on-a-chip technology. A neural stem cell (NSC) spheroid and human umbilical vein endothelial cells (HUVECs) were mixed with extracellular matrix (ECM) from a microfluidic chip, loaded onto the chip, and then cultured. First, we demonstrated the differentiation of stem cells and the characteristics of angiogenesis. Then, we introduced proinflammatory cytokines to the chip to replicate the early development of the brain during an inflammatory process and studied the changes in angiogenesis and neurogenesis. Lastly, we preliminarily demonstrated the inhibitory effect of ibuprofen on neuroinflammation. The contribution of this work is as follows: (1) for the first time, we visualized the early characteristics of angiogenesis and NSC differentiation under neuroinflammation in a short culture cycle; (2) we revealed the changes in the neurovascular unit structure and neurovascular coupling under neuroinflammation; (3) we investigated the outcomes of using ibuprofen to reduce neuroinflammation at the cell-tissue level. This work has the potential to greatly enhance our understanding of the early progression of neurodevelopmental disorders caused by neuroinflammation and provides a valuable reference for the development of therapeutic strategies for neuroinflammation during the neurodevelopmental period.

2 Materials and methods

2.1 Fabrication of the microfluidic chips

Physiologically, neurodevelopment and angiogenesis in the brain are synchronous and interactive [29, 30] (Fig. 1a). To model neurovascular development in the embryonic brain, we designed a microfluidic chip containing a central channel for the ECM with neural spheroid and endothelial cells and two lateral/side channels for the culture medium (Figs. 1b and 1c). Two parallel rows of micropillars separated the side channels from the central channel to prevent ECM leakage, and the distance between adjacent micropillars was 100 μm. The central channel was 1.3 mm in width, the lateral channels were 1.0 mm in width, and all channels were 150 μm in depth (Fig. S1 in the supplementary information).

The microfluidic chip was fabricated using lithography technology and consisted of two layers: a glass slide bottom layer and a polydimethylsiloxane (PDMS) top layer. The PDMS base and curing agent (SYLGARD 184; Dow Corning, USA) were mixed at a 10:1 (mass fraction) ratio to obtain the PDMS prepolymer, which was then poured into a silicon master. After degassing in a vacuum dryer for approximately 15 min, the master containing the PDMS prepolymer was placed in a drying oven at 80 °C for approximately 60 min. The PDMS layer was then cut from the master using a scalpel, taped to remove dust, and punched with a microfluidic hole puncher (Zhongding Yuxuan New Material Technology Co., Ltd., Hefei, China; hole diameter for ECM: 1.8 mm; hole diameter for medium: 4.0 mm). Finally, an oxygen plasma processor was used to bond the PDMS layer to the glass slide to obtain the microfluidic chip, which was stored overnight in a drying oven at 80 °C to enhance bonding. Before being used in the experiments, the microfluidic chip was wrapped in aluminum foil and autoclaved at 121 °C for 60 min.

2.2 Cell culture

HUVECs were purchased from Wuhan PriCells Company and cultured in endothelial cell medium (1001; ScienCell, USA) in T-25 cell culture flasks (430639; Corning, USA). HUVECs between Passages 5 and 10 were used in this study. To facilitate visualization of angiogenesis, before the experiments, the HUVECs were transduced with lentivirus constructs to express red fluorescence. Mouse neural stem cells (NE-4Cs) [31–34] were purchased from the National Collection of Authenticated Cell Cultures and cultured in minimum essential medium (MEM; 11090-081; Gibco, USA) supplemented with 1% GlutaMAX (35050061; Gibco), 1% sodium pyruvate (11360070; Gibco), 1% non-essential amino acids (11140050; Gibco), 10% fetal bovine serum (Life Science, Australia), and 0.1% mycoplasma prevention reagent (FM501-01; TransGen, China). Cells were maintained in a 37 °C and 5% CO_2 humid cell incubator (Forma 3131; Thermo, USA). We chose to use HUVECs and NE-4Cs because HUVECs are widely used to form neurovascular networks [35] and NE-4Cs are widely used to differentiate into various neural microtissues [31–34].

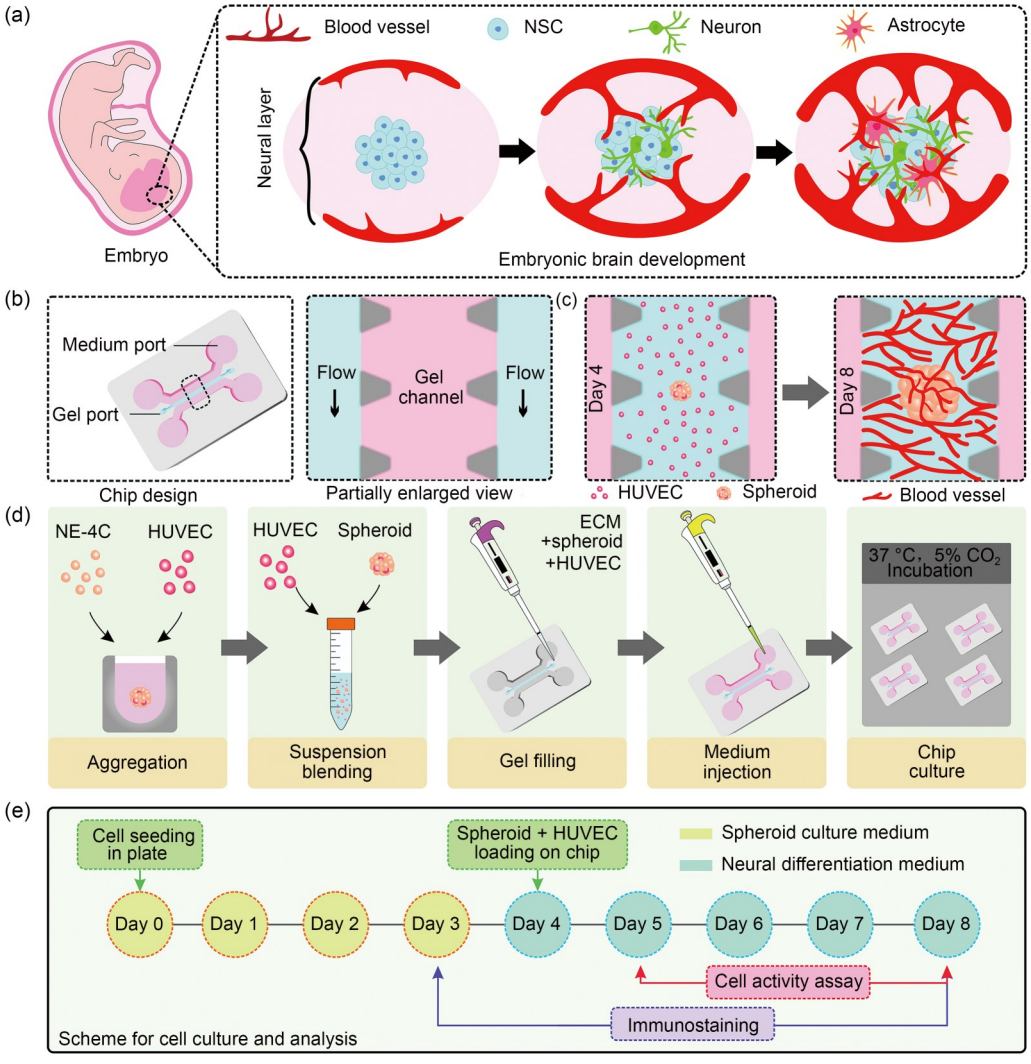

Fig. 1 Modeling neurovascular development on a microfluidic chip. (a) Schematic of neurovascular development in the embryonic brain. (b) Schematic of the developed microfluidic chip. (c) Schematic of neurovascularization on the chip. (d) Schematic of experiments for modeling neurovascular development on the chip. (e) Schematic of cell culture and analysis

2.3 Cell pre-staining assay

To facilitate visualization of cell growth, before the experiments, NE-4Cs were incubated at 37 °C for 30 min with 3,3'-dioctadecyloxacarbocyanine perchlorate dye (DiO; C1993S; Beyotime, China) to express green fluorescence in the dark. After incubation, the cells were washed three times with Dulbecco's phosphate-buffered saline (D-PBS). Experiments related to these pre-stained cells should be performed in the dark.

2.4 Preparation of the prevascularized neural spheroids

Previous studies have shown that using endothelial cells with neural spheroids can improve vascularization and reduce apoptosis at the center of the spheroids [35]. Thus, in this study, prevascularized neural spheroids were prepared. To obtain cell spheroids with an initially matched size, the operation conditions for forming the spheroids (i.e., cell number, medium volume, incubation time, etc.) were kept strictly the same. In brief, NE-4Cs were trypsinized by the addition of 0.05% trypsin-ethylenediaminetetraacetic acid (EDTA) solution (25300054; Gibco) for 2 min and then centrifuged at 150*g* for 5 min. After centrifugation, the supernatant was discarded, and the NE-4Cs were resuspended in a fresh cell culture medium [36]. HUVECs were trypsinized using 0.25% trypsin-EDTA solution (25300056; Gibco), centrifuged at 200*g* for 5 min, and resuspended as described above. After cell counting, the HUVEC suspension was mixed with the NE-4C suspension (the adopted ratio of HUVECs to NE-4Cs was 1:10 according to the reported study [35]). Then, the mixed cells were seeded into a

round-bottom low-attachment 96-well plate (7007; Corning) and centrifuged at 200*g* for 10 min (ST40R; Thermo Fisher Scientific, USA) to better aggregate the cells in each well into a spheroid. The cells in the 96-well plates were cultured for at least 3 d in a humidified incubator at 37 °C and 5% CO_2 to obtain prevascularized neural spheroids (Fig. S2 in the supplementary information). When the diameter of the spheroids reached approximately 70 μm (the diameter was calculated by the arithmetical mean of the maximum and minimum lengths of the spheroids) [37], the spheroids were carefully collected into a centrifuge tube and then centrifuged at 200*g* for 5 min. After the supernatant was removed, the spheroids were resuspended in a small quantity of culture medium for use in the subsequent experiments.

To promote the growth of neural spheroids in the plate, spheroid cultural medium (SCM; a mixture of endothelial cell medium and MEM supplemented with 1% GlutaMAX, 1% sodium pyruvate, 1% non-essential amino acids, and 0.1% mycoplasma prevention reagent) was used in the early stages of spheroid culture.

2.5 Loading of neural spheroids and cells

In this study, fibrinogen conjugated with thrombin was used as the ECM because it can promote cell adhesion and proliferation in brain chips, according to previous studies [38, 39]. Fibrinogen (20430ES03; Yeasen, China) and thrombin (20402ES03; Yeasen) from bovine plasma were separately dissolved in 0.9% NaCl solution and sterilized using a 0.22-μm filter (Millex; Millipore, USA). First, the suspension of HUVECs was well mixed with the fibrinogen solution and the solution of neural spheroids (the density of HUVECs was approximately 5×10^6 cells/mL, and the final concentration of fibrinogen was 3.0 mg/mL) [16]. After mixing with the thrombin solution (the final concentration of thrombin was 3 U/mL), the mixture was quickly loaded into the central channel of the microfluidic chip using a pipette. It is important to note that the microfluidic chip and the pipette tips used in the experiments should be precooled to −20 °C, and the loading process should be performed on ice. Then, the microfluidic chip was placed in a humid cell incubator at 37 °C for 15 min to allow fibrinogen polymerization. Finally, a pipette was used to gently load the fresh cell culture medium into the medium channel, and four cut sterile pipette tips were inserted into the inlet and outlet of the medium channels, respectively, to serve as medium reservoirs. The chip was placed in a sterile box containing a small amount of sterile water and cultured in a 37 °C and 5% CO_2 humid cell incubator (Fig. 1d). The culture medium was refreshed every day.

To promote the growth and differentiation of neural spheroids on the chip [35], neural differentiation medium (NDM; a mixture of ECM and MEM supplemented with 1% GlutaMAX, 1% sodium pyruvate, 1% non-essential amino acids, 2% B27 (17504044; Gibco), 1% N-2 (17502048; Gibco), and 0.1% mycoplasma prevention reagent) was used during chip culture. The reservoirs on one side of the medium channel were filled with NDM, while those on the other side were filled with NDM-V (NDM containing vascular endothelial growth factor (VEGF; 50 ng/mL; AF-100-20-100; PeproTech, USA)).

We observed the growth of the NVU on Days 4, 6, and 8 and examined the differentiation by immunofluorescence staining on Day 8, while the cell activity analyses were performed on Day 5 (24 h after the loading of HUVECs and NE-4C spheroids) and Day 8. In addition, to observe the small and rapid changes in vascularization, we examined the tapered tips of the angiogenic sprouts on Day 7.

2.6 Experiments on neuroinflammation-induced neurodevelopmental disorders

To model neuroinflammation-induced neurodevelopmental disorders in the chip, tumor necrosis factor-alpha (TNF-α, P00029; Solarbio, China) and interleukin-6 (IL-6, P00022; Solarbio) proinflammatory cytokines were used based on previous studies [40]. When the chip had been cultured for 24 h, the cell culture medium was replaced with a medium containing TNF-α (final concentration: 1 ng/mL) and IL-6 (final concentration: 1 ng/mL). Then, the chip was cultured for a further 24 h.

2.7 Anti-inflammatory control

Ibuprofen is a nonsteroidal anti-inflammatory drug (NSAID) widely used for its anti-inflammatory, antipyretic, and analgesic properties [41]. As an anti-inflammatory drug for preterm neonates, ibuprofen may be a potential therapeutic candidate for treating brain injury caused by neuroinflammation [42]. The use of ibuprofen should be avoided starting from the fifth month of gestation [43]. Our study can only be used to verify the validity of the anti-inflammatory effect and does not support the use of ibuprofen in the treatment of neuroinflammation during pregnancy. Ibuprofen (II0020; Solarbio) was added to the culture medium at a working concentration of 50 μg/mL on Day 5. After 72 h, we tested the effects of different concentrations of ibuprofen on the growth and development of the neural spheroids and then selected the working concentration, which was also supported by previous studies [44], for the subsequent experiments (Figs. S3 and S4 in the supplementary information).

2.8 Immunofluorescence staining

For immunofluorescence staining on the chip (Fig. 1e), first, the two lateral medium channels on the chip were slowly

injected with D-PBS solution for 5 min to remove any impurity (hereafter referred to as the washing step), and cells were fixed with 4% formaldehyde for 12 h at 4 °C. Next, the chip was washed with 0.05% PBST solution (PBS containing 0.05% Tween 20) for 15 min and then treated with 0.1% Triton X-100 solution (PBS containing 0.1% Triton X-100) for 30 min to improve the permeability of the cell membranes. After washing with PBST for 15 min, the chip was blocked with 2% bovine serum albumin in PBS at 4 °C overnight. After incubation with the primary antibody for 8 h at 4 °C, the chip was stained with the secondary antibody in the dark for 40 min at room temperature, and the cell nuclei were stained with 4',6-diamidino-2-phenylindole (DAPI) dye (C1002; Beyotime). After washing with PBST to remove the unbound dyes, the chip was imaged under an inverted fluorescence microscope (IX73; Olympus, Japan) or a confocal laser scanning microscope (FV1000; Olympus). The primary and secondary antibodies used were as follows: cluster of differentiation 31 (CD31) rabbit polyclonal antibody (347526; ZENBIO, China), glial fibrillary acidic protein (GFAP, 9A2) mouse monoclonal antibody (250027; ZENBIO), beta III tubulin rabbit monoclonal antibody (R23620; ZENBIO), SRY-box transcription factor 2 (SOX2) rabbit polyclonal antibody (11064-1-AP; Proteintech, China), nestin rabbit polyclonal antibody (19483-1-AP; Proteintech), zonula occludens 1 (ZO1) polyclonal antibody (21773-1-AP; Proteintech), laminin beta 1 polyclonal antibody (23498-1-AP; Proteintech), smooth muscle actin (SMA) polyclonal antibody (14395-1-AP; Proteintech), goat anti-rabbit immunoglobulin G (IgG, H&L)-Alexa Fluor 594 (550043; ZENBIO), goat anti-rabbit IgG (H&L)-Alexa Fluor 488 (550037; ZENBIO), goat anti-mouse IgG (H&L)-Alexa Fluor 594 (550042; ZENBIO), and goat anti-mouse IgG (H&L)-Alexa Fluor 488 (550036; ZENBIO).

For cytoskeleton staining, after the cells on the chip were fixed and permeabilized as described above, the cells were incubated with Actin-Tracker dyes (C2201S and C2205S; Beyotime) for 20 min in the dark at room temperature, and the cell nuclei were stained with DAPI dyes.

2.9 Enzyme-linked immunosorbent assay (ELISA) analysis

To test the protein level on the chip during culture (Fig. 1e), the culture medium was collected from the microfluidic chip every day during chip culture and centrifuged at 200*g* for 20 min to remove cell debris, and the supernatant was stored at −80 °C for use. The concentrations of TNF-α and IL-6 were analyzed using ELISA kits (JL20268 and JL10484; Jianglaibio, China) according to the manufacturer's instructions. A microplate reader was used to immediately measure the absorption of each sample at 450 nm. The levels of TNF-α and IL-6 were calculated using a calibration curve based on the known concentration. This experiment was carried out in triplicate.

2.10 Cell activity analysis

The viability of the cells on the chip was analyzed using cell staining (Fig. 1e). In brief, the chip was washed with D-PBS for 5 min and then incubated for 20 min in the dark at 37 °C with calcein acetoxymethyl ester (calcein-AM, C2012; Beyotime) and propidium iodide (PI, ST511; Beyotime) to stain living and dead cells, respectively. The fluorescence images of the cells were captured using an inverted fluorescence microscope. ImageJ software was used to count the number of living and dead cells.

The proliferation ability of the cells on the chip was evaluated using an Alamar Blue kit (BB-4206; BestBio, China). The chip was incubated with 10% Alamar Blue solution in the culture medium for 12 h in a humid cell incubator. After incubation, the medium was collected and the absorbance at 495 nm was immediately measured using a microplate reader.

2.11 Blood vessel analysis

Blood vessels within a 300-μm radius of the boundary of the neural spheroid on the microfluidic chip were included in the statistical range. The microvessel density was calculated using the Vessel J plugin (Health Sciences Center, McMaster University, Canada), and the number of vascular nodes, the number of vascular branches, the length of the vascular branch, and the number of angiogenic sprouts that entered the neural spheroid were counted or measured using ImageJ software. The microvascular network coverage at the edge of the neural spheroid was calculated as the ratio of the projection distance on the spheroidal circumference of the capillary fused with the spheroid to the circumference of the neural spheroid.

2.12 Neural differentiation analysis

The numbers of neurons and astrocytes were counted based on the immunofluorescence images using ImageJ software. The length of the neural axon, the thickness of the neuron layer, and the quantification of the fluorescence intensity in the immunofluorescence images were measured using ImageJ software.

2.13 Reverse transcription-quantitative polymerase chain reaction (RT-qPCR)

RNA was isolated using TRI-reagent (BS258A; Biosharp, China) following the manufacturer's instructions. Reverse

transcription was conducted using the Hifair II 1st Strand cDNA Synthesis Kit (11119ES60; Yeasen), and qPCR was conducted using SYBR Green qPCR Mix (BL698A; Biosharp). RT-qPCR was performed using the QuantStudio 3 real-time PCR system (3 min at 95 °C followed by 40 cycles (15 s at 95 °C; 30 s at 60 °C)). The expression of *IL-1β*, *IL-6*, *IL-10*, *IL-10RA*, *IL-13*, *IL-18*, *TNF-α*, transforming growth factor-beta (*TGF-β*), and C-X-C motif chemokine ligand 10 (*CXCL10*) was normalized to the expression of the housekeeping gene glyceraldehyde-3-phosphate dehydrogenase (*GAPDH*) [11].

2.14 Statistical analysis

In this study, in each experiment, at least three NVU chips were used. GraphPad Prism software was used for data analysis and mapping. Data were presented as mean±standard deviation. *P*-values were analyzed using a two-tailed Student's *t*-test or one-way analysis of variance (ANOVA). The significance levels are indicated by $^{*}p<0.05$, $^{**}p<0.01$, and $^{***}p<0.001$, and N.S. for no significance.

3 Results

3.1 Construction of the NVU-on-a-chip

To model embryonic brain development, a prevascularized neural spheroid was cocultured with HUVECs on a microfluidic chip. During culture, the size of the neural spheroids gradually increased with the proliferation of cells, while the spherical shape and structural integrity were maintained (Fig. 2a). Some NE-4Cs migrated to the peripheral ECM of the spheroid, and the HUVECs elongated and self-assembled into a microvascular network around the neural spheroid (Fig. 2b; please note that due to the obstruction of neural cells and the strong fluorescence contrast between the inside and outside of the neural spheroids, the

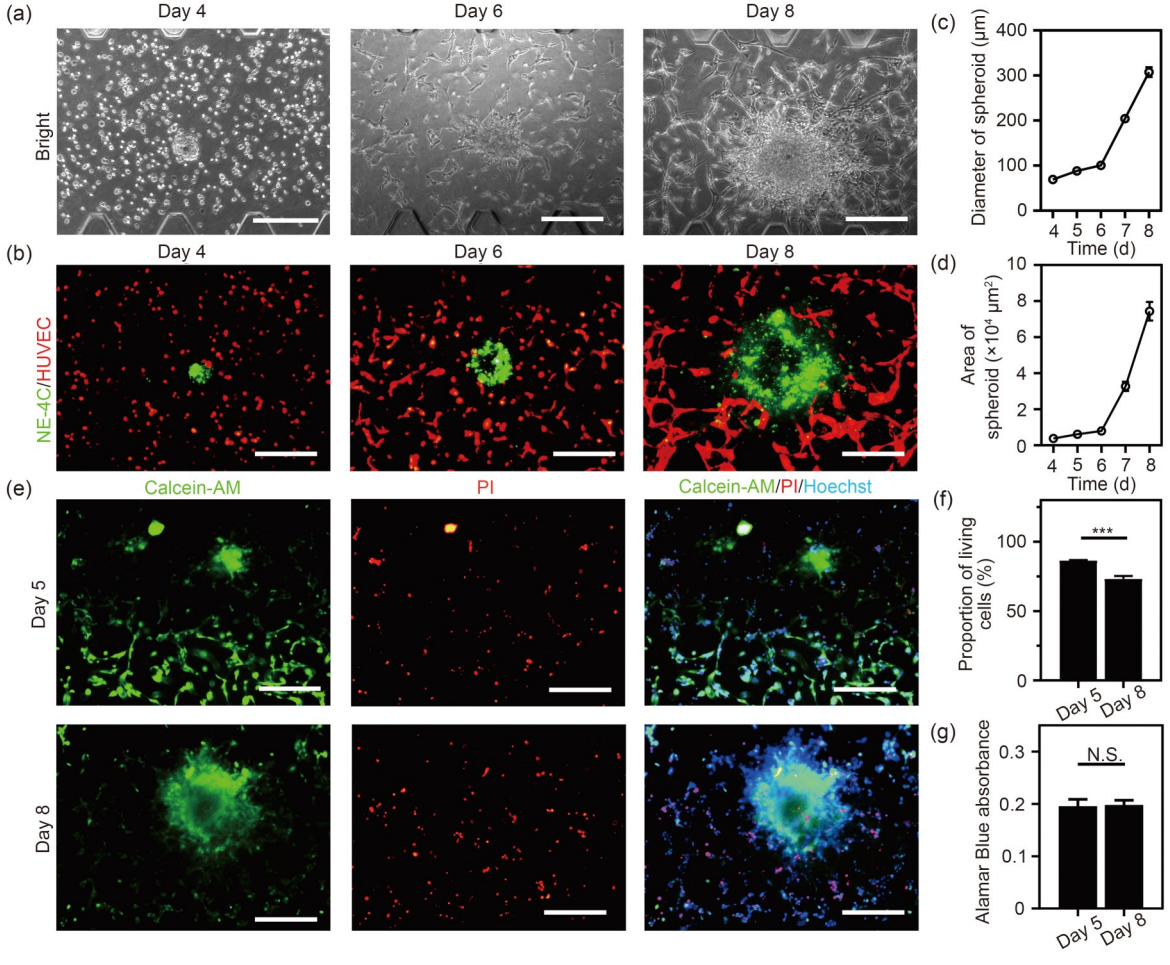

Fig. 2 Construction of the NVU-on-a-chip. (a) Bright-field images of the vascularized neural spheroids on the chip on Days 4, 6, and 8. (b) Fluorescence images of the vascularized neural spheroids on the chip on Days 4, 6, and 8 (NE-4Cs are green and HUVECs are red). (c) Diameter of the neural spheroids (n=5). (d) Area of the neural spheroids (n=5). (e) Fluorescence images of cells stained with calcein-AM (green), PI (red), and Hoechst 33342 (blue) on Days 5 and 8. (f) Proportion of living cells (n=3). (g) Analysis of cell proliferation (n=3). Scale bar: 200 μm. Data are expressed as mean±standard deviation. $^{***}p<0.001$. N.S.: no significance

red fluorescence of the HUVECs inside the pre-spheroids looks weak; the pre-vascularization can be observed more clearly in Fig. S2 in the supplementary information). The statistical results revealed that the increase in the diameter (Fig. 2c) or the area (Fig. 2d) of the spheroid was relatively slow at the early stage of culture (i.e., from Day 4 to Day 6) but was rapid at the later stage of culture (i.e., from Day 6 to Day 8), which may be due to the limited height of the chip. To evaluate cell viability, cells on the chip were stained with calcein-AM and PI dyes (Fig. 2e; Fig. S5 in the supplementary information). The results showed that as NE-4Cs and HUVECs proliferated rapidly, the proportion of living cells decreased slightly (Fig. 2f), possibly as a result of the limited supply of nutrients; however, the proliferation ability of the cells was maintained (Fig. 2g).

3.2 Mimicked vascularization of the embryonic brain on the chip

The vascularization of the human embryonic brain is a highly complex process. Recent studies have confirmed that neural spheroids obtained by coculturing NSCs with HUVECs can recapitulate embryonic neocortical development and may serve as a platform to investigate neurovascular diseases and injuries [35, 45]. To characterize the vascularization of the neural spheroid on the chip, the neurons were stained with beta III, while the capillaries were stained with SMA (Fig. 3a). The results showed that the periphery of the neural spheroid was surrounded by abundant capillaries, reflecting the cerebral cortex wrapped by the pial capillary anastomotic plexus at the early stage of embryonic development [46]. In the cell culture plates where the neural spheroids were cocultured with HUVECs, a few cells in the spheroids differentiated into neurons, suggesting that the chip significantly promoted the association of neural spheroids with endothelial cells (Fig. S6 in the supplementary information). We also constructed 3D images to exhibit the spatial distribution characteristics of the formed microvascular network (Fig. 3b). Interestingly, compared to the microvascular network without neural spheroids (Fig. S7 in the supplementary information), the capillaries cocultured with neural spheroids had smaller diameters and shorter branches (Fig. S8 in the supplementary information), similar to the situation in vivo, verifying the role of astrocytes in constructing capillaries [16].

The characteristics in the three stages of vascularization were well recapitulated and were similar to the real physiological vascularization process in vivo [46]. The characteristics were as follows:

(1) At the early stage, endothelial cells were in close contact with the periphery of spheroids (Fig. 3c), indicating the fusing stage where capillaries contact with the cortex external glial limiting membrane (EGLM) with fusion of the vascular and glial basal laminae [46].

(2) In the middle stage, the spheroid was invaded by the tapered tips of angiogenic sprouts (Fig. 3d), indicating the inserting stage where the filopodium of the endothelium is inserted into the fused laminae and then gradually enters into the nervous tissue [46]. The morphology of the endothelial cells was similar to that of the tip cells, which are a subtype of endothelial cells that are highly enriched near the active neurogenesis zone [47]. This phenomenon also agreed with the results presented in Fig. 3a.

(3) At the final stage, the whole capillary penetrated into the nervous tissue (Fig. S9 in the supplementary information), indicating the penetrating stage where the whole capillary penetrates into the cortex and establishes an extravascular Virchow–Robin compartment [46].

To quantify the progression of vascularization at different developmental stages, the coverage rate of the microvascular network around the neural spheroid (for evaluating the efficiency of capillaries fusing with neural tissue) was calculated (Fig. 3e), and the number of angiogenic sprouts that entered into the neural spheroid (for evaluating the efficiency of capillary inserting into neural tissue) was counted (Fig. 3f). The results showed that without external intervention (i.e., inflammation-induced neurodevelopmental disorders), the angiogenesis process progressed uniformly, and the neural spheroids showed abundant vascularization characteristics after five days.

3.3 Differentiation of the NSC spheroids on the chip

To confirm the differentiation status of the neural spheroids, the expression of specific biomarkers was analyzed. Before loading of the spheroid, in the cell culture plate, neural stem cells inside the spheroid were undifferentiated (nestin and SOX2, two neural stem cell markers, were detected, as shown in Figs. 4a and 4b), whereas after loading and culturing on the chip, they were differentiated into astrocytes and neurons (GFAP, a specific biomarker of astrocytes, and beta III, a specific biomarker of neurons, were observed, as shown in Fig. 4c and Fig. S10 in the supplementary information). In addition, compared with the neural spheroids cultured off the chip (Fig. 4d), the edges of the spheroids on the chip turned from clear and smooth to irregular due to cell migration and differentiation (Fig. 4e).

To show the degree of differentiation of the neural spheroids on the chip, the intensities of beta III (Fig. 4f) and GFAP (Fig. 4g) fluorescence were measured. The specific expression of both proteins was very low on Day 3, but high on Day 8 (comparatively, in the plate, the expression of both proteins was extremely low on both Day 3

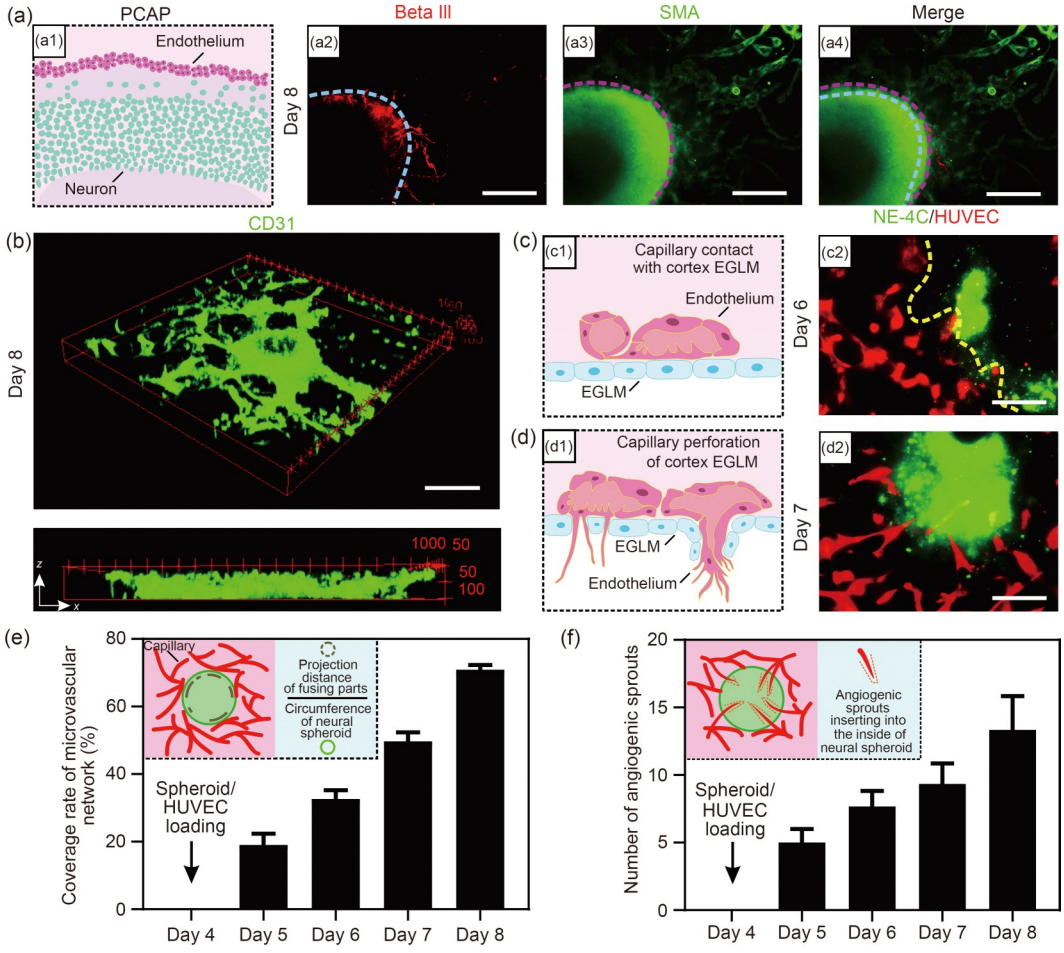

Fig. 3 Vascularization of the embryonic brain mimicked with the chip. (a) Schematic of the pial capillary anastomotic plexus (PCAP) covering the cerebral cortex during embryonic development and fluorescence images of cells stained with SMA (green) and beta III (red) on Day 8. Scale bar: 200 μm. (b) Three-dimensional reconstruction of the microvascular network on Day 8. Scale bar: 100 μm. (c) Schematic of pial capillary contacting and fusing with the cortex EGLM and fluorescence image of HUVECs (red) and NE-4Cs (green) on Day 6. Scale bar: 100 μm. (d) Schematic of endothelium filopodium penetrating through the fused laminae and entering the nervous tissue and fluorescence image of HUVECs (red) and NE-4Cs (green) on Day 7. Scale bar: 100 μm. (e) Coverage rate of the microvascular network. (f) Number of angiogenic sprouts. Data are expressed as mean±standard deviation (n=3)

and Day 8; Figs. S6 and S11 in the supplementary information), further confirming that the five-day on-chip culture promoted the differentiation of neural spheroids. We also reconstructed 3D images of GFAP and beta III to show the spatial distribution of astrocytes and neurons (Fig. 4h), and the images suggested the establishment of a complex patterned architecture linking astrocytes and neurons.

3.4 Engineered inflammation-induced neurodevelopmental disorders using the NVU-on-a-chip

Recently, a damaging inflammatory response has been detected in brains with perinatal injuries such as FGR [48–50], hypoxic-ischemic encephalopathy [8], and cerebral palsy [9], which has been proven to be directly related to neuronal damage and reduced permeability of the BBB [51, 52] (Fig. 5a).

To engineer inflammation-induced neurodevelopmental disorders on the chip, two proinflammatory cytokines, TNF-α and IL-6 [53], were introduced on Day 5 (Fig. 5b). Before the introduction (i.e., on Day 4), the NI (neuroinflammation) and IBU (ibuprofen; a promising drug for neuroinflammation [54]) groups expressed similar levels of inflammation. After 24 h of exposure to low-dose inflammatory stimuli, the concentration of proinflammatory cytokines increased significantly, suggesting that we successfully modeled the inflammatory response in the early neurodevelopment period (some previous studies showed changes in IL-6 in the serum of pregnant women with FGR [55, 56]; in this study, the changing trend of IL-6 was consistent with the conclusion from the placental tissue of FGR [57, 58]). In the IBU group, the concentrations of

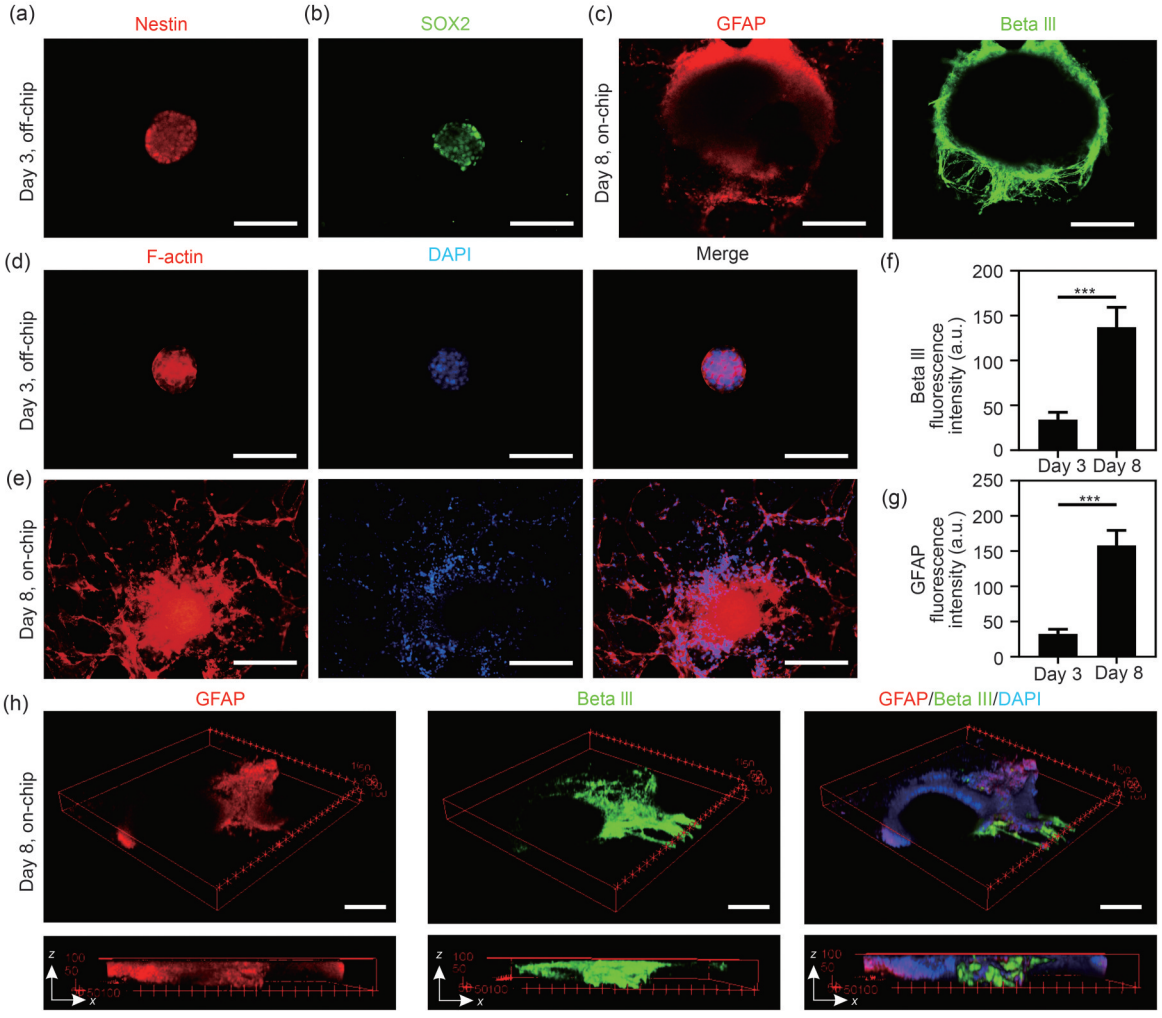

Fig. 4 Differentiation of the NSC spheroid on the chip. (a) Fluorescence image of the neural spheroid stained with nestin (red) in the plate on Day 3. Scale bar: 100 μm. (b) Fluorescence image of the neural spheroid stained with SOX2 (green) in the plate on Day 3. Scale bar: 100 μm. (c) Fluorescence images of neural spheroids stained with GFAP (red) and beta III (green) on the chip on Day 8. Scale bar: 100 μm. (d) Fluorescence images of the cytoskeleton (red) and cell nucleus (blue) in the plate on Day 3. Scale bar: 100 μm. (e) Fluorescence images of the cytoskeleton (red) and cell nucleus (blue) on the chip on Day 8. Scale bar: 200 μm. (f) Statistics of beta III fluorescence intensity on Days 3 and 8. (g) Statistics of GFAP fluorescence intensity on Days 3 and 8. (h) Three-dimensional reconstruction of the chip. The cells were stained with GFAP (red), beta III (green), and DAPI (blue). Scale bar: 200 μm. Data are expressed as mean±standard deviation (n=3). $^{***}p<0.001$

TNF-α (Fig. 5c) and IL-6 (Fig. 5d) presented a downward trend, suggesting that ibuprofen has good anti-inflammatory ability (it should be noted that because NE-4Cs and HUVECs come from different species, the coculture caused the secretion of a certain quantity of proinflammatory cytokines (Fig. S12 in the supplementary information) and consequently, it is infeasible to set the group without inflammation). To further confirm the engineered inflammation-induced disorders, we also validated the changes in gene expression (i.e., *IL-1β*, *IL-10RA*, *IL-18*, *TNF-α*, and *TGF-β*) associated with inflammation modeling via RT-qPCR (Fig. S13 in the supplementary information).

In terms of the proportion of living cells (Fig. 5e; untreated group in Fig. 2f) and the proliferation of cells (Fig. 5f; untreated group in Fig. 2g), the anti-inflammatory ability of ibuprofen was also confirmed. The images (Fig. 5g) showed that inflammation also affected the outward migration of NE-4Cs (Figs. 5h and 5i; untreated groups in Figs. 2c and 2d) and the assembly of the microvascular network, verifying the inhibitory activity of neuroinflammation on fetal or neonatal brain size, which is the simplest and most intuitive indicator for clinical judgment of growth restricted fetuses [7]. Here, we aimed to construct an in vitro model for replicating the basic features of inflammation-induced neurodevelopmental disorders in the early period and then replacing conventional animal models rather than studying the changes in cytokines. Therefore, the changes in cytokines before and after drug delivery need to be studied in depth in the future.

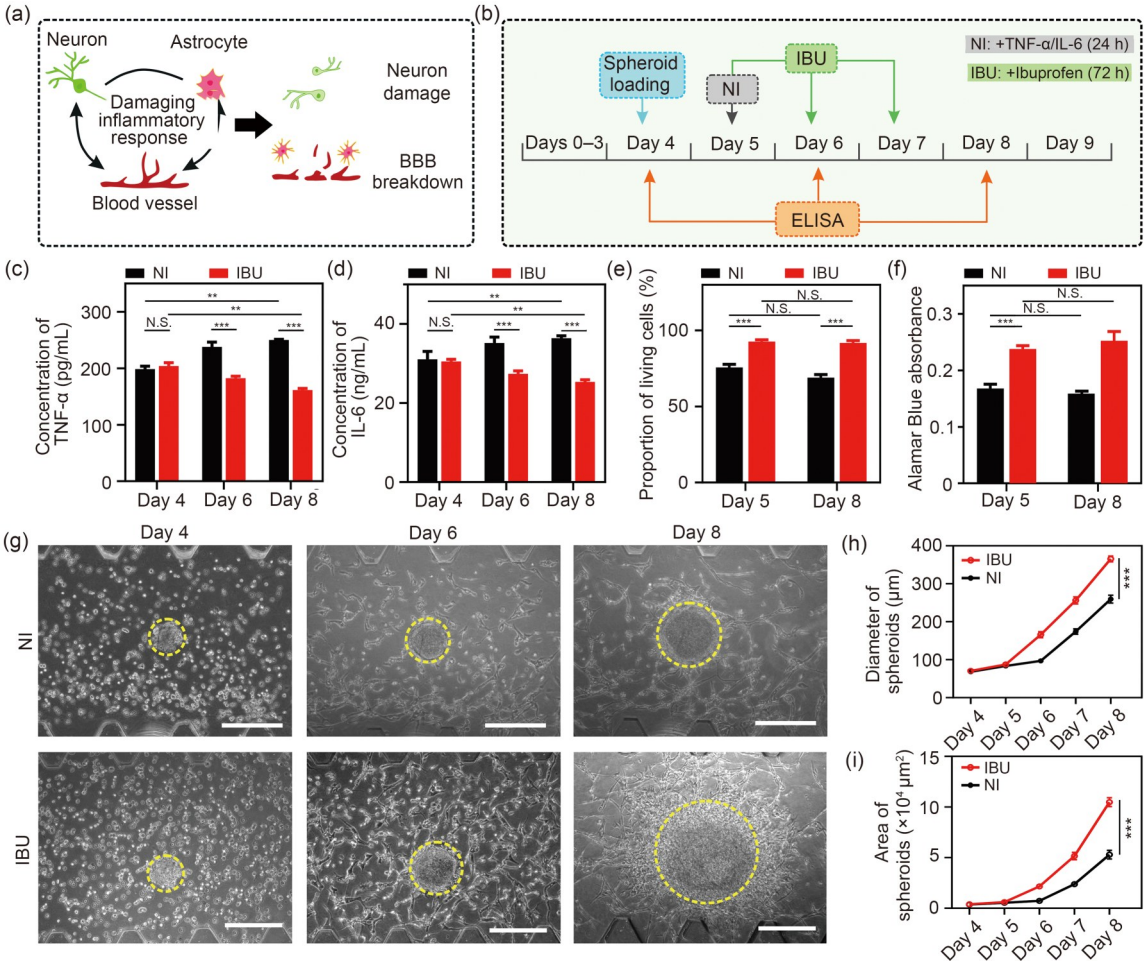

Fig. 5 Engineered inflammation-induced neurodevelopmental disorders using the NVU-on-a-chip. (a) Schematic of the neuroinflammation-induced neurodevelopmental disorder. (b) Scheme of the construction and treatment of neuroinflammation. (c) Statistics of the concentration of TNF-α (n=3). (d) Statistics of the concentration of IL-6 (n=3). (e) Statistics of the proportion of living cells (n=3). (f) Statistics of cellular proliferation (n=3). (g) Bright-field images of the development of neural spheroids under neuroinflammation (NI) and ibuprofen (IBU) on Days 4, 6, and 8. Scale bar: 200 μm. (h) Statistics of the spheroid diameters under NI and IBU (n=5). (i) Statistics of the spheroid areas under NI and IBU (n=5). Data are expressed as mean±standard deviation. $^{**}p<0.01$; $^{***}p<0.001$. N.S.: no significance

3.5 Microvascular changes under neuroinflammation

To demonstrate the effect of neuroinflammation on angiogenesis, we compared the microvascular morphologies between the NI and IBU groups on Day 8 (Fig. 6a). Under neuroinflammation, the coverage of the neural spheroid by the microvascular network was decreased (Fig. 6b; untreated group in Fig. 3e), and the number of angiogenic sprouts entering the interior of the spheroid was reduced (Fig. 6c; untreated group in Fig. 3f). The results confirmed that neuroinflammation significantly disrupted the fusing and inserting stages of vascularization (i.e., inhibiting angiogenesis), and that the timely anti-inflammatory administration of drugs such as IBU could remedy this situation. Under neuroinflammation, the microvessels were slender and hardly formed a stable connection (Fig. 6d). In the case of IBU administration, the density of the microvessels (Fig. 6e), the number of vascular nodes (Fig. 6f), and the number of branches around the spheroid (Fig. 6g) increased significantly. In addition, using the method proposed in the literature [59], we found that the tight junctions between cells were greatly reduced under neuroinflammation (Figs. 6h and 6i), which may cause BBB leakage [60, 61].

3.6 Neural cell changes under neuroinflammation

To demonstrate the effects of neuroinflammation on differentiated astrocytes and neurons, we compared the neurovascular units in the NI and IBU groups. Under neuroinflammation, the astrocytes were sharp and scattered between the capillaries (Fig. 7a), whereas under IBU administration, the astrocytes were regular (Fig. 7b) and capillaries were

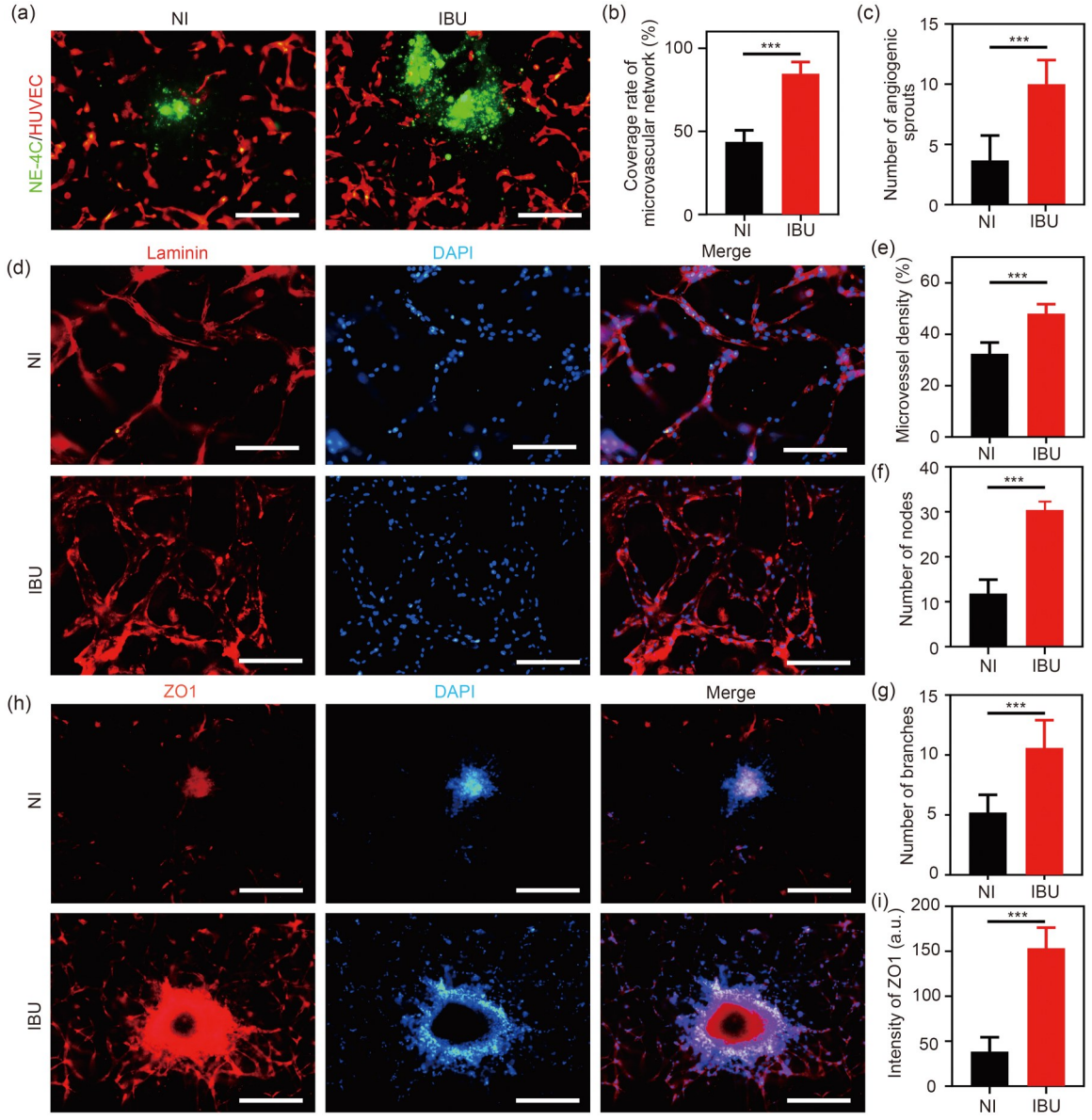

Fig. 6 Neurovascular changes under neuroinflammation. (a) Fluorescence images of HUVECs (red) and NE-4Cs (green) on Day 8. Scale bar: 200 μm. (b) Statistics of the coverage rate of microvascular networks under NI and IBU on Day 8. (c) Statistics of the number of angiogenic sprouts under NI and IBU on Day 8. (d) Immunofluorescence images of on-chip cells stained with laminin (red) and DAPI (blue) dyes on Day 8. Scale bar: 100 μm. (e) Statistics of the microvessel density. (f) Statistics of the number of vascular nodes. (g) Statistics of the number of vascular branches. (h) Immunofluorescence images of on-chip cells stained with ZO1 (red) and DAPI (blue) dyes on Day 8. Scale bar: 200 μm. (i) Statistics of the ZO1 fluorescence intensity. Data are expressed as mean±standard deviation (n=3). $^{***}p<0.001$

wrapped around the spheroids (Fig. 7c, which infers the position of astrocytes and capillaries, according to the method proposed in [16]). The results indicated that neuroinflammation disrupted the structure of the neurovascular units, causing astrocytes to lose their ability to regulate the capillaries. Neuroinflammation also led to a significant increase in the differentiation of NSCs into astrocytes (Figs. 7d and 7e), which is similar to the inflammatory response of glial cells found in vivo [11, 62].

Under neuroinflammation, the neurons were shriveled and hollowed (Fig. 7f), whereas under IBU administration, dense and clear neurons were observed (Fig. 7g). In addition, the axons in the IBU group extended along the branches of the blood vessels and were curved at the bifurcations of the capillaries (Fig. 7h), whereas those in the NI group were shorter (Fig. 7i). This phenomenon revealed the disruption of the interaction between neurons and capillaries by neuroinflammation and validated the guidance of capillaries to axon localization [63–65]. We also replicated neuron damage, manifested as changed morphology (Fig. 7g), a decreased number of neurons (Fig. 7j), and reduced thickness of the neuron layer (Fig. 7k). It should be noted that

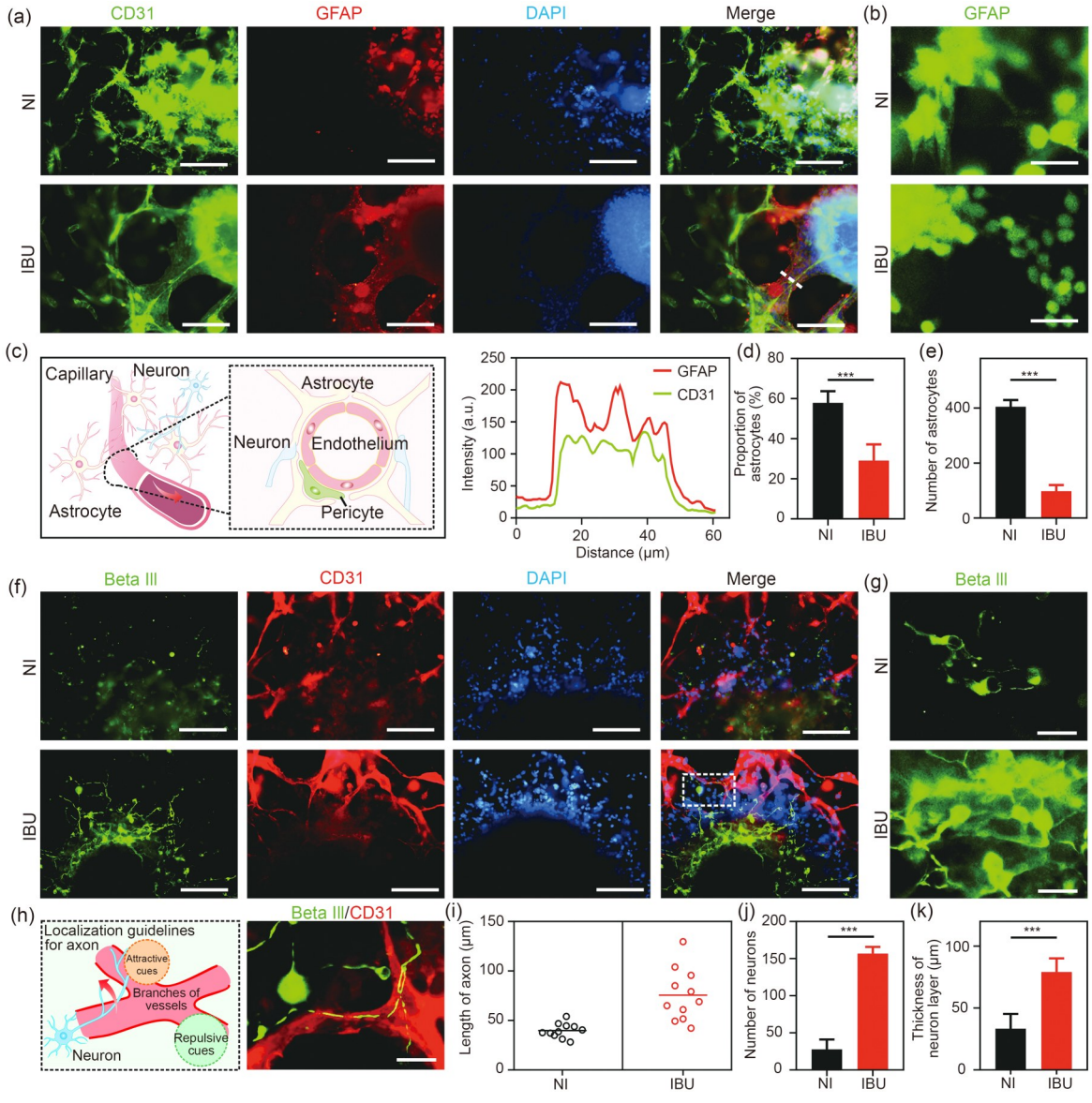

Fig. 7 Neural cell changes under neuroinflammation. (a) Immunofluorescence images of on-chip cells stained with CD31 (green), GFAP (red), and DAPI (blue) dyes on Day 8. Scale bar: 200 μm. (b) Immunofluorescence images of astrocytes stained with GFAP (green). Scale bar: 10 μm. (c) Schematic of the neurovascular unit and fluorescence intensity of GFAP and CD31 at the position indicated by the white line in Fig. 7a. (d) Statistics of the proportion of astrocytes. (e) Statistics of the number of astrocytes. (f) Fluorescence images of on-chip cells stained with beta III (green), CD31 (red), and DAPI (blue) dyes on Day 8. Scale bar: 100 μm. (g) Immunofluorescence images of neurons stained with beta III (green). Scale bar: 10 μm. (h) Schematic of the localization guidelines of neural axon development and immunofluorescence image of cells stained with beta III (green) and CD31 (red) at the position indicated by the white box in Fig. 7f. (i) Statistics of the length of neural axons. (j) Statistics of the number of neurons. (k) Statistics of the thickness of the neuron layer. Data are expressed as mean±standard deviation (n=3). $^{***}p<0.001$

although we used NE-4Cs and HUVECs on the chip, the obtained phenomena were similar to the results from animal models with neuroinflammation [11, 14, 15].

4 Discussion

Neurodevelopmental disorder is a slowly progressive and restrictive disease [66–68]. In the early stages of neural development, brain injuries are usually undetectable in vivo; thus, the inflammation-caused changes in vascularization and the differentiation of neural stem cells during the early neurodevelopment period remain unclear. In this study, for the first time, we attempted to model a neuroinflammation-induced neurodevelopmental disorder on a self-developed NVU-on-a-chip.

In the clinic, neuroinflammation is a signature of many neurodevelopmental disorders [3]. In this study, our model

expressed highly similar disease features to those in animal models with neuroinflammation [11–13], including proinflammatory cytokine upregulation, astrocyte activation and proliferation, neuron damage, and capillary injury. Thus, our model was able to replicate some features of perinatal brain injury related to neuroinflammation.

Brain sections from animal models can only provide structural information about the brain in the postpartum period. In contrast, our chip is a novel platform for real-time, dynamic visualization of disease progression during early development, providing rich and exact information on neuroinflammation treatment at the cell-tissue level. Our findings revealed the detailed features of angiogenesis and the interactions between the neurovascular units under pathological and normal states. In addition, our results suggested that small inflammatory stimuli may lead to neurodevelopmental disorders at the early stage of embryonic brain development, and that timely anti-inflammatory intervention with ibuprofen may effectively improve neurodevelopmental outcomes. It should be noted that although the ECM (fibrinogen conjugated with thrombin) we adopted promotes angiogenesis, it may also increase the risk of neuroinflammation [69, 70]. However, according to a previous study [39], the inflammatory cytokines induced by the ECM are negligible compared with the inflammatory levels in this study.

For the on-chip neurodevelopmental disorder we modeled, there is space for optimization. First, due to the limited source of human brain cells, mouse neural stem cells and HUVECs were adopted; consequently, some phenomena may have been missed due to the cross-species coculture of cells. In future work, human pluripotent stem cell-derived neural cells and endothelial cells (even neural organoids) should be used. Thus, the functions of other neural cells (such as oligodendrocytes and microglia) and cerebral microvessels can be determined [71, 72]. Second, it is currently challenging to spontaneously form a perfusable microvascular network in a complex coculture system [73]. To better simulate brain development on a microfluidic chip, a solution for forming perfusable microvascular networks needs to be proposed. Third, to simplify the experiments, we examined only the morphology of differentiated neural cells under neuroinflammation. By integrating the microelectrodes on the chip, the electrophysiological function and BBB integrity of the NVU-on-a-chip can be deeply evaluated [16, 74–77]. Fourth, based on a previous study [22], we quantified only typical inflammatory cytokines in the neurodevelopmental disorder. In future work, more cytokines and/or changes in gene expression will be analyzed to consolidate our findings and to discover other mechanisms of neurodevelopmental disorders.

5 Conclusions

In this study, we modeled an inflammation-induced neurodevelopmental disorder using a self-developed NVU-on-a-chip, visualized the features of neurodevelopment, and presented the outcomes of anti-inflammatory intervention with ibuprofen. The results revealed that neuroinflammation hindered the expansion of neural spheroids and inhibited the angiogenic process, leading to astrocyte activation and proliferation, neuron damage, and capillary injury. Neuroinflammation also disrupted the interactions between capillaries and neurons/astrocytes, resulting in damage to the neurovascular unit and neurovascular coupling failure. This study lays a foundation for discovering the early-stage progression of neurodevelopmental disorders.

Supplementary Information The online version contains supplementary material available at https://doi.org/10.1631/bdm.2400107.

Acknowledgements This work was partially supported by the National Key R&D Program of China (No. 2018AAA0100300), the National Natural Science Foundation of China (Nos. 82072018, 82274375, and 82402490), the Anhui Provincial Science and Technology Major Project (No. 202203a07020006), the Strategic Priority Research Program (C) of the Chinese Academy of Sciences (CAS) (No. XDC07040200), the Key R&D Program of Anhui Province (No. 2022e07020012), the Natural Science Foundation of Anhui Province (No. 2208085QH256), the Fundamental Research Funds for the Central Universities (No. WK2100000042), and the China Postdoctoral Science Foundation (No. 2022M713055). This work was partially carried out at the USTC Center for Micro and Nanoscale Research and Fabrication.

Author contributions RZ: investigation, methodology, data curation, formal analysis, writing, revising, and editing; ZDS: methodology, data curation, revising, editing, and validation; CPL: formal analysis, methodology, writing, and funding acquisition; FX: methodology and funding acquisition; XCZ: methodology; XFD: methodology and validation; DBH: supervision and funding acquisition; BSQ: supervision, funding acquisition, and methodology; WPD: conceptualization, supervision, funding acquisition, methodology, revising, and editing.

Declarations

Conflict of interest The authors declare that they have no conflict of interest.

Ethical approval This study does not contain any studies with human or animal subjects performed by any of the authors.

Data availability The data that support the findings of this study are available from the corresponding authors upon reasonable request.

References

1. Corps KN, Roth TL, McGavern DB (2015) Inflammation and neuroprotection in traumatic brain injury. JAMA Neurol 72(3): 355–362. https://doi.org/10.1001/jamaneurol.2014.3558

2. Goshi N, Morgan RK, Lein PJ et al (2020) A primary neural cell culture model to study neuron, astrocyte, and microglia interactions in neuroinflammation. J Neuroinflammation 17(1): 155. https://doi.org/10.1186/s12974-020-01819-z
3. Han VX, Patel S, Jones HF et al (2021) Maternal immune activation and neuroinflammation in human neurodevelopmental disorders. Nat Rev Neurol 17(9):564–579. https://doi.org/10.1038/s41582-021-00530-8
4. Simon DW, McGeachy MJ, Bayır H et al (2017) The far-reaching scope of neuroinflammation after traumatic brain injury. Nat Rev Neurol 13(3):171–191. https://doi.org/10.1038/nrneurol.2017.13
5. Obermeier B, Daneman R, Ransohoff RM (2013) Development, maintenance and disruption of the blood–brain barrier. Nat Med 19(12):1584–1596. https://doi.org/10.1038/nm.3407
6. Lee HG, Lee JH, Flausino LE et al (2023) Neuroinflammation: an astrocyte perspective. Sci Transl Med 15(721):eadi7828. https://doi.org/10.1126/scitranslmed.adi7828
7. Miller SL, Huppi PS, Mallard C (2016) The consequences of fetal growth restriction on brain structure and neurodevelopmental outcome. J Physiol 594(4):807–823. https://doi.org/10.1113/JP271402
8. Ranjan AK, Gulati A (2023) Advances in therapies to treat neonatal hypoxic-ischemic encephalopathy. J Clin Med 12(20): 6653. https://doi.org/10.3390/jcm12206653
9. Calado CMS, Manhães-de-Castro R, Pereira S et al (2023) Therapeutic advances for treating memory impairments in perinatal brain injuries with implications for cerebral palsy: a systematic review and meta-analysis of preclinical studies. Exp Neurol 365: 114411. https://doi.org/10.1016/j.expneurol.2023.114411
10. Kelly SB, Tran NT, Polglase GR et al (2023) A systematic review of immune-based interventions for perinatal neuroprotection: closing the gap between animal studies and human trials. J Neuroinflammation 20(1):241. https://doi.org/10.1186/s12974-023-02911-w
11. Wixey JA, Sukumar KR, Pretorius R et al (2019) Ibuprofen treatment reduces the neuroinflammatory response and associated neuronal and white matter impairment in the growth restricted newborn. Front Physiol 10:541. https://doi.org/10.3389/fphys.2019.00541
12. Alves de Alencar Rocha AK, Allison BJ, Yawno T et al (2017) Early- versus late-onset fetal growth restriction differentially affects the development of the fetal sheep brain. Dev Neurosci 39(1–4):141–155. https://doi.org/10.1159/000456542
13. Sutherland AE, Yawno T, Castillo-Melendez M et al (2020) Does antenatal betamethasone alter white matter brain development in growth restricted fetal sheep? Front Cell Neurosci 14: 100. https://doi.org/10.3389/fncel.2020.00100
14. Bell A, Watt AP, Dudink I et al (2023) Endothelial colony forming cell administration promotes neurovascular unit development in growth restricted and appropriately grown fetal lambs. Stem Cell Res Ther 14(1):29. https://doi.org/10.1186/s13287-023-03249-z
15. Wixey JA, Lee KM, Miller SM et al (2019) Neuropathology in intrauterine growth restricted newborn piglets is associated with glial activation and proinflammatory status in the brain. J Neuroinflammation 16(1):5. https://doi.org/10.1186/s12974-018-1392-1
16. Campisi M, Shin Y, Osaki T et al (2018) 3D self-organized microvascular model of the human blood–brain barrier with endothelial cells, pericytes and astrocytes. Biomaterials 180:117–129. https://doi.org/10.1016/j.biomaterials.2018.07.014
17. Cui BF, Cho SW (2022) Blood–brain barrier-on-a-chip for brain disease modeling and drug testing. BMB Rep 55(5):213–219. https://doi.org/10.5483/BMBRep.2022.55.5.043
18. Marino A, Tricinci O, Battaglini M et al (2018) A 3D real-scale, biomimetic, and biohybrid model of the blood–brain barrier fabricated through two-photon lithography. Small 14(6):1702959. https://doi.org/10.1002/smll.201702959
19. Jagtiani E, Yeolekar M, Naik S et al (2022) In vitro blood brain barrier models: an overview. J Contr Release 343:13–30. https://doi.org/10.1016/j.jconrel.2022.01.011
20. Brandl S, Reindl M (2023) Blood–brain barrier breakdown in neuroinflammation: current in vitro models. Int J Mol Sci 24(16):12699. https://doi.org/10.3390/ijms241612699
21. Bhatia SN, Ingber DE (2014) Microfluidic organs-on-chips. Nat Biotechnol 32(8):760–772. https://doi.org/10.1038/nbt.2989
22. Pediaditakis I, Kodella KR, Manatakis DV et al (2022) A microengineered Brain-Chip to model neuroinflammation in humans. iScience 25(8):104813. https://doi.org/10.1016/j.isci.2022.104813
23. Lyu ZL, Park J, Kim KM et al (2021) A neurovascular-unit-on-a-chip for the evaluation of the restorative potential of stem cell therapies for ischaemic stroke. Nat Biomed Eng 5(8):847–863. https://doi.org/10.1038/s41551-021-00744-7
24. Vatine GD, Barrile R, Workman MJ et al (2019) Human iPSC-derived blood–brain barrier chips enable disease modeling and personalized medicine applications. Cell Stem Cell 24(6):995–1005.e6. https://doi.org/10.1016/j.stem.2019.05.011
25. Peng B, Hao SP, Tong ZQ et al (2022) Blood–brain barrier (BBB)-on-a-chip: a promising breakthrough in brain disease research. Lab Chip 22(19):3579–3602. https://doi.org/10.1039/d2lc00305h
26. Wang YQ, Wang L, Zhu YJ et al (2018) Human brain organoid-on-a-chip to model prenatal nicotine exposure. Lab Chip 18(6): 851–860. https://doi.org/10.1039/c7lc01084b
27. Cui KL, Wang YQ, Zhu YJ et al (2020) Neurodevelopmental impairment induced by prenatal valproic acid exposure shown with the human cortical organoid-on-a-chip model. Microsyst Nanoeng 6:49. https://doi.org/10.1038/s41378-020-0165-z
28. Barreras P, Pamies D, Hartung T et al (2023) Human brain microphysiological systems in the study of neuroinfectious disorders. Exp Neurol 365:114409. https://doi.org/10.1016/j.expneurol.2023.114409
29. Paredes I, Himmels P, de Almodóvar CR (2018) Neurovascular communication during CNS development. Dev Cell 45(1):10–32. https://doi.org/10.1016/j.devcel.2018.01.023
30. Carmeliet P, Tessier-Lavigne M (2005) Common mechanisms of nerve and blood vessel wiring. Nature 436(7048):193–200. https://doi.org/10.1038/nature03875
31. Nascimento L, Fernandes C, Silva RM et al (2023) Customizing 3D structures of vertically aligned carbon nanotubes to direct neural stem cell differentiation. Adv Healthc Mater 12(26): e2300828. https://doi.org/10.1002/adhm.202300828
32. Li XD, Zhou DZ, Jin ZZ et al (2020) A coaxially extruded heterogeneous core–shell fiber with Schwann cells and neural stem cells. Regen Biomater 7(2):131–139.

https://doi.org/10.1093/rb/rbz037
33. Li HY, Li SJ, Ren CH et al (2022) Hypoxic postconditioning promotes neurogenesis by modulating the metabolism of neural stem cells after cerebral ischemia. Exp Neurol 347:113871. https://doi.org/10.1016/j.expneurol.2021.113871
34. Gao L, Li PP, Shao TY et al (2020) Neurotoxic role of interleukin-17 in neural stem cell differentiation after intracerebral hemorrhage. Neur Regen Res 15(7):1350–1359. https://doi.org/10.4103/1673-5374.272614
35. Shi YC, Sun L, Wang MD et al (2020) Vascularized human cortical organoids (vOrganoids) model cortical development in vivo. PLoS Biol 18(5):e3000705. https://doi.org/10.1371/journal.pbio.3000705
36. Shin N, Kim Y, Ko J et al (2022) Vascularization of iNSC spheroid in a 3D spheroid-on-a-chip platform enhances neural maturation. Biotechnol Bioeng 119(2):566–574. https://doi.org/10.1002/bit.27978
37. Li CP, Li SB, Du K et al (2021) On-chip replication of extremely early-stage tumor behavior. ACS Appl Mater Interfaces 13(17): 19768–19777. https://doi.org/10.1021/acsami.1c03740
38. Ahn SI, Sei YJ, Park HJ et al (2020) Microengineered human blood–brain barrier platform for understanding nanoparticle transport mechanisms. Nat Commun 11(1):175. https://doi.org/10.1038/s41467-019-13896-7
39. Hajal C, Offeddu GS, Shin Y et al (2022) Engineered human blood–brain barrier microfluidic model for vascular permeability analyses. Nat Protoc 17(1):95–128. https://doi.org/10.1038/s41596-021-00635-w
40. Wimmer RA, Leopoldi A, Aichinger M et al (2019) Human blood vessel organoids as a model of diabetic vasculopathy. Nature 565(7740):505–510. https://doi.org/10.1038/s41586-018-0858-8
41. Kantor TG (1979) Ibuprofen. Ann Intern Med 91(6):877–882. https://doi.org/10.7326/0003-4819-91-6-877
42. Wixey JA, Chand KK, Pham L et al (2018) Therapeutic potential to reduce brain injury in growth restricted newborns. J Physiol 596(23):5675–5686. https://doi.org/10.1113/JP275428
43. Leverrier-Penna S, Michel A, Lecante LL et al (2021) Exposure of human fetal kidneys to mild analgesics interferes with early nephrogenesis. FASEB J 35(7):e21718. https://doi.org/10.1096/fj.202100050R
44. Cucullo L, Couraud PO, Weksler B et al (2008) Immortalized human brain endothelial cells and flow-based vascular modeling: a marriage of convenience for rational neurovascular studies. J Cereb Blood Flow Metab 28(2):312–328. https://doi.org/10.1038/sj.jcbfm.9600525
45. Ahn Y, An JH, Yang HJ et al (2021) Human blood vessel organoids penetrate human cerebral organoids and form a vessel-like system. Cells 10(8):2036. https://doi.org/10.3390/cells10082036
46. Marín-Padilla M (2012) The human brain intracerebral microvascular system: development and structure. Front Neuroanat 6: 38. https://doi.org/10.3389/fnana.2012.00038
47. Crouch EE, Bhaduri A, Andrews MG et al (2022) Ensembles of endothelial and mural cells promote angiogenesis in prenatal human brain. Cell 185(20):3753–3769.e18. https://doi.org/10.1016/j.cell.2022.09.004
48. Zinni M, Pansiot J, Colella M et al (2021) Impact of fetal growth restriction on the neonatal microglial proteome in the rat. Nutrients 13(11):3719. https://doi.org/10.3390/nu13113719
49. Fleiss B, Van Steenwinckel J, Bokobza C et al (2021) Microglia-mediated neurodegeneration in perinatal brain injuries. Biomolecules 11(1):99. https://doi.org/10.3390/biom11010099
50. Fleiss B, Wong F, Brownfoot F et al (2019) Knowledge gaps and emerging research areas in intrauterine growth restriction-associated brain injury. Front Endocrinol 10:188. https://doi.org/10.3389/fendo.2019.00188
51. Olmos G, Lladó J (2014) Tumor necrosis factor alpha: a link between neuroinflammation and excitotoxicity. Mediators Inflamm 2014:861231. https://doi.org/10.1155/2014/861231
52. Cheng YY, Desse S, Martinez A et al (2018) TNFα disrupts blood brain barrier integrity to maintain prolonged depressive-like behavior in mice. Brain Behav Immun 69:556–567. https://doi.org/10.1016/j.bbi.2018.02.003
53. Irimia D, Wang X (2018) Inflammation-on-a-chip: probing the immune system ex vivo. Trends Biotechnol 36(9):923–937. https://doi.org/10.1016/j.tibtech.2018.03.011
54. Padilla N, Alexandrou G, Blennow M et al (2015) Brain growth gains and losses in extremely preterm infants at term. Cereb Cortex 25(7):1897–1905. https://doi.org/10.1093/cercor/bht431
55. Bartha JL, Romero-Carmona R, Comino-Delgado R (2003) Inflammatory cytokines in intrauterine growth retardation. Acta Obstet Gynecol Scand 82(12):1099–1102. https://doi.org/10.1046/j.1600-0412.2003.00259.x
56. Raghupathy R, Al-Azemi M, Azizieh F (2012) Intrauterine growth restriction: cytokine profiles of trophoblast antigen-stimulated maternal lymphocytes. Clin Dev Immunol 2012: 734865. https://doi.org/10.1155/2012/734865
57. Street ME, Seghini P, Fieni S et al (2006) Changes in interleukin-6 and IGF system and their relationships in placenta and cord blood in newborns with fetal growth restriction compared with controls. Eur J Endocrinol 155(4):567–574. https://doi.org/10.1530/eje.1.02251
58. Kiyokoba R, Uchiumi T, Yagi M et al (2022) Mitochondrial dysfunction-induced high hCG associated with development of fetal growth restriction and pre-eclampsia with fetal growth restriction. Sci Rep 12(1):4056. https://doi.org/10.1038/s41598-022-07893-y
59. Winkelman MA, Kim DY, Kakarla S et al (2021) Interstitial flow enhances the formation, connectivity, and function of 3D brain microvascular networks generated within a microfluidic device. Lab Chip 22(1):170–192. https://doi.org/10.1039/d1lc00605c
60. Keaney J, Campbell M (2015) The dynamic blood–brain barrier. FEBS J 282(21):4067–4079. https://doi.org/10.1111/febs.13412
61. Evans LE, Taylor JL, Smith CJ et al (2021) Cardiovascular comorbidities, inflammation, and cerebral small vessel disease. Cardiovasc Res 117(13):2575–2588. https://doi.org/10.1093/cvr/cvab284
62. Boche D, Gerhard A, Rodriguez-Vieitez E et al (2019) Prospects and challenges of imaging neuroinflammation beyond TSPO in Alzheimer's disease. Eur J Nucl Med Mol Imaging 46(13):2831–2847. https://doi.org/10.1007/s00259-019-04462-w
63. Lowery LA, Van Vactor D (2009) The trip of the tip: understanding the growth cone machinery. Nat Rev Mol Cell Biol 10(5):332–343. https://doi.org/10.1038/nrm2679
64. Segarra M, Aburto MR, Hefendehl J et al (2019) Neurovascular interactions in the nervous system. Annu Rev Cell Dev Biol 35: 615–635.

https://doi.org/10.1146/annurev-cellbio-100818-125142
65. Suter TACS, Jaworski A (2019) Cell migration and axon guidance at the border between central and peripheral nervous system. Science 365(6456):eaaw8231. https://doi.org/10.1126/science.aaw8231
66. Audette MC, Kingdom JC (2018) Screening for fetal growth restriction and placental insufficiency. Semin Fetal Neonatal Med 23(2):119–125. https://doi.org/10.1016/j.siny.2017.11.004
67. Nardozza LMM, Caetano ACR, Zamarian ACP et al (2017) Fetal growth restriction: current knowledge. Arch Gynecol Obstet 295(5):1061–1077. https://doi.org/10.1007/s00404-017-4341-9
68. Monet MC, Quan N (2023) Complex neuroimmune involvement in neurodevelopment: a mini-review. J Inflamm Res 16: 2979–2991. https://doi.org/10.2147/JIR.S410562
69. Iannucci J, Grammas P (2023) Thrombin, a key driver of pathological inflammation in the brain. Cells 12(9):1222. https://doi.org/10.3390/cells12091222
70. Wen TT, Zhang ZH (2023) Cellular mechanisms of fibrin (ogen): insight from neurodegenerative diseases. Front Neurosci 17:1197094. https://doi.org/10.3389/fnins.2023.1197094
71. Brites D, Fernandes A (2015) Neuroinflammation and depression: microglia activation, extracellular microvesicles and microRNA dysregulation. Front Cell Neurosci 9:476. https://doi.org/10.3389/fncel.2015.00476
72. Au NPB, Ma CHE (2022) Neuroinflammation, microglia and implications for retinal ganglion cell survival and axon regeneration in traumatic optic neuropathy. Front Immunol 13:860070. https://doi.org/10.3389/fimmu.2022.860070
73. O'Connor C, Brady E, Zheng Y et al (2022) Engineering the multiscale complexity of vascular networks. Nat Rev Mater 7(9):702–716. https://doi.org/10.1038/s41578-022-00447-8
74. Kagan BJ, Kitchen AC, Tran NT et al (2022) In vitro neurons learn and exhibit sentience when embodied in a simulated game-world. Neuron 110(23):3952–3969.e8. https://doi.org/10.1016/j.neuron.2022.09.001
75. Leng YB, Li XR, Zheng FY et al (2023) Advances in in vitro models of neuromuscular junction: focusing on organ-on-a-chip, organoids, and biohybrid robotics. Adv Mater 35(41):2211059. https://doi.org/10.1002/adma.202211059
76. Nashimoto Y, Hayashi T, Kunita I et al (2017) Integrating perfusable vascular networks with a three-dimensional tissue in a microfluidic device. Int Biol 9(6):506–518. https://doi.org/10.1039/c7ib00024c
77. Wang YI, Abaci HE, Shuler ML (2017) Microfluidic blood–brain barrier model provides in vivo-like barrier properties for drug permeability screening. Biotechnol Bioeng 114(1):184–194. https://doi.org/10.1002/bit.26045